Terahertz Few-particle Magnetoabsorption in Asymmetric Ellipsoidal Ge/Si QD

© A.A. Nahapetyan[1], M.A. Mkrtchyan[1,2,¶], M.Ya. Vinnichenko[3], D.A. Firsov[3], H.A. Sarkisyan[1]

[1] Institute of Applied Problems of Physics National Academy of Sciences of the Republic of Armenia,
0014 Yerevan, Armenia
[2] Russian-Armenian University,
0051 Yerevan, Armenia
[3] Peter the Great St. Petersburg Polytechnic University,
195251 St. Petersburg, Russia
¶ E-mail: mher.mkrtchyan@rau.am

Received October 20, 2025
Revised November 21, 2025
Accepted December 12, 2025

The behavior of a heavy-hole gas in a strongly oblate, asymmetric ellipsoidal Ge/Si quantum dot under an axial homogeneous magnetic field has been investigated. Due to the specific geometry of the quantum dot, the interaction between holes is considered two-dimensional. The realization of the generalized Kohn theorem in such a system under the influence of the incident long-wave radiation has been shown in the dipole approximation. The exact energy spectrum has been obtained for the case of a strongly oblate ellipsoidal quantum dots with a circular cross-section, using the Johnson and Payne model of a circular two-dimensional parabolic well. A detailed analysis of the energy spectrum is presented.

Keywords: ellipsoidal quantum dot, magnetic field, Moshinsky model, generalized Kohn theorem, terahertz optical transitions, Johnson and Payne model.

DOI: 10.61011/SC.2025.09.62834.8676

1. Introduction

Quantum dots are unique objects whose physical properties can be manipulated by changing their geometrical sizes, the component compositions, and their geometrical shapes. By their properties, QDs, in various aspects, are identical to real atoms, due to a fully quantized spectrum of charge carriers. This enables the application of various quantum-mechanical methods for describing real atomic systems, clarifying the peculiarities of physical processes in QDs [1–7]. The QD interaction with various types of radiation can provide important information about the specificity of the zone structure construction of the investigated compounds and the possibility of their application as active functional media in the new generation of semiconductor devices [8–11]. The greater the geometrical complexity of the QD, the more geometrical parameters characterize its energy spectrum. Therefore, the flexible manipulation of the energy spectrum can be performed in such systems, allowing the system to be tuned to predetermined physical characteristics, such as the resonant frequencies of interband and intraband absorptions, as well as current parameters, among others [12–14]. Unlike real atoms, the interaction of QD with external electromagnetic radiation can induce the optical transitions within the conduction band or in the valence band, so between the levels of the conduction and valence bands. As the energy spectra of both electrons and holes are very sensitive to the change of QD geometrical parameters, it is clear that the resonant frequencies of the corresponding transitions will strongly depend on the above-mentioned parameters of QD as well [15–17]. One of the interesting optical effects identified in QDs is connected with the specific character of long-wave intraband absorption in QDs with parabolic confinement, containing a pair-interacting gas of charge carriers. In the articles [18–20], it has been shown that the resonant frequencies of the long-wave transitions in such systems don't depend on the number of particles, hence on the interaction between them. The given statement is named after the generalized Kohn theorem and is a generalization of the original Kohn theorem [21], which states that the cyclotron resonance of long-wave radiation in a pair- interacting gas of charged particles in an axial magnetic field doesn't depend on the interaction between those particles. In the works [22–25], it has been shown that the generalized Kohn theorem is realized in QDs with lens-shaped and ellipsoidal geometries of strongly oblate and strongly prolate shapes. The theoretical justification of that statement is based on the possibility of adiabatic description of the electron or hole gas behavior in the ellipsoidal or the lens-shaped QDs with strongly oblate or prolate geometries. Based on the adiabatic method, it was shown that the slow subsystem is confined by the parabolic effective confining potential, and the magnitude of the interaction potential energy between the particles of a gas depends only on the modulus of the distance between them. The calculations that were carried out for the case of the plano-convex lens-shaped Ge/Si QD containing pair-interacting heavy hole gas gave good coincidence with experimental results [25]. It has been shown that the energy of the resonant transitions

corresponds to the terahertz range of radiation. In recent work [26] has been investigated the possibility of realization of the generalized Kohn theorem in the fully asymmetric QD when all the semiaxes are not equal to each other, in particular, the possibility of implementation of the two-dimensional Moshinsky model [27–29] for the analytical description of the long-wave absorption in the mentioned system has been shown. It should be mentioned that the application of an axial magnetic field can become an additional mechanism for the manipulation of the resonant frequencies of long-wave transitions.

This paper is a logical conclusion to the previous articles and aims to investigate:

• the influence of the magnetic field on the long-wave absorption in the strongly oblate asymmetric ellipsoidal QD,

• the implementation of the exactly solvable Johnson-Payne model for the analytical description of the heavy hole gas behavior in the strongly oblate QD with the circular cross-section in the presence of an axial magnetic field, and the demonstration of the generalized Kohn theorem in the considered system.

2. Theory

Consider a strongly oblate asymmetric ellipsoidal quantum dot (SOAEQD) containing a few-particle heavy hole gas in the presence of an axial homogeneous magnetic field B. The strong oblateness is defined by the following inequalities: $c/a \ll 1$, $c/b \ll 1$, where a, b, c are semiaxes of the ellipsoid in the OX, OY and OZ directions, respectively (Figure 1).

We suppose that the confining potential is described in the framework of the infinite-deep-walls model:

$$V_{\text{conf}}(\mathbf{r}_i) = \begin{cases} 0, \dfrac{x_i^2}{a^2} + \dfrac{y_i^2}{b^2} + \dfrac{z_i^2}{c^2} \le 1, \\ \infty, \dfrac{x_i^2}{a^2} + \dfrac{y_i^2}{b^2} + \dfrac{z_i^2}{c^2} > 1. \end{cases} \tag{1}$$

The interparticle interaction is assumed to be dependent only on the mutual distance between the particles:

$$V_{\text{int}}(\mathbf{r_1}, \dots \mathbf{r}_N) = \frac{1}{2} \sum_{\substack{i=1 \\ j \ne 1}}^{N} \sum_{j=1}^{N} v(|\mathbf{r}_i - \mathbf{r}_j|). \tag{2}$$

The Hamiltonian of the considered system has the following form:

$$H = \frac{1}{2\mu} \sum_{i=1}^{N} \left(\mathbf{p}_i - \frac{e}{c} \mathbf{A}_i \right)^2 + \sum_{i=1}^{N} V_{\text{conf}}(\mathbf{r}_i) + V_{\text{int}}(\mathbf{r}_i, \dots, \mathbf{r}_N), \tag{3}$$

where $\mu = 0.39 m_0$ is the heavy hole effective mass in Ge/Si [23].

Turn to the consideration of the given system in the framework of the adiabatic approximation. As was shown in the papers [22–24], the wave function of the system can be presented in the form of the product of wave functions, describing the fast subsystem $\psi_{\text{f}}(z_1; (x_1, y_1), \dots, z_N; (x_N, y_N))$ and the slow subsystem $\psi_s(x_1, \dots, x_N; y_1, \dots, y_N)$.

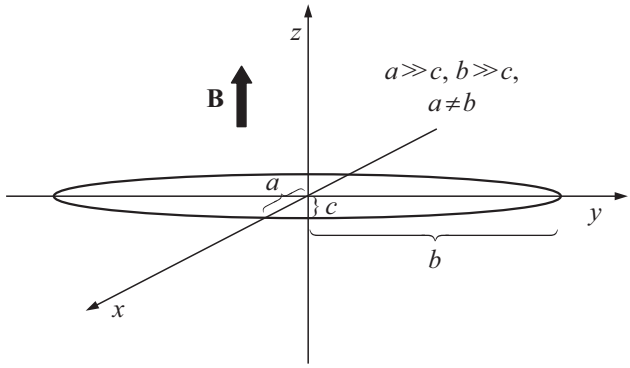

Figure 1. Strongly oblate asymmetric ellipsoidal Ge/Si QD.

$$\Psi(\mathbf{r}_1, \dots, \mathbf{r}_N) = \psi_{\text{f}}(z_1; (x_1, y_1), \dots, z_N; (x_N, y_N)) \times \psi_s(x_i, \dots, x_N; y_1, \dots, y_N). \tag{4}$$

According to the article [26], the wave function and the energy of the fast subsystem, which parametrically depend on the coordinates of the slow subsystem, have these forms:

$$\begin{cases} E_{n_z}^z(x_1, \dots, x_N; y_1, \dots, y_N) = \sum\limits_{i=1}^{N} \dfrac{\pi^2 \hbar^2 n_{z_i}^2}{2\mu L^2(x_i, y_i)}, \\ \psi_{\text{f}}(z_1; (x_1, y_1), \dots, z_N; (x_N, y_N)) = \\ \quad = \prod\limits_{i=1}^{N} \sqrt{\dfrac{2}{L(x_1, y_1)}} \sin\left(\dfrac{\pi n_{z_i}}{L(x_i, y_y)} z_i + \delta_{n_{z_i}} \right). \end{cases} \tag{5}$$

Based on the adiabatic approach, similar to [26], it can be shown that the slow subsystem is described with the two-dimensional many-particle Schrodinger equation of the form:

$$\left[\sum_{i=1}^{N} \left(\frac{1}{2\mu} (p_{x_i}^2 + p_{y_i}^2) + \frac{\omega_c}{2} (y_i p_{x_i} - x_i p_{y_i}) + \frac{\mu}{2} (\Omega_x^2 x_i^2 + \Omega_y^2 y_i^2) \right) + V_{\text{int}}^{\text{2D}}(\boldsymbol{\rho}_1, \dots, \boldsymbol{\rho}_N) \right] \times \psi_s(x_i, \cdot, x_N; y_1, \dots, y_N) = \text{E} \psi_s(x_1, \dots, x_N; y_1, \dots, y_N), \tag{6}$$

where

$$\text{E} \equiv \left(E - N \frac{\pi^2 \hbar^2}{8\mu c^2} \right), \quad \omega_c = eB/\mu c$$

is the cyclotron resonance frequency,

$$\Omega_{x(y)}^2 \equiv \left(\Omega_{a(b)}^2(1) + \frac{1}{4} \omega_c^2 \right),$$

with $\Omega_a(1) = \pi\hbar/2\mu ac$, and $\Omega_b(1) = \pi\hbar/2\mu bc$ [26]. It is assumed that the interaction between particles has a

two-dimensional character, as the size quantization in the axial direction is significantly stronger compared to the interparticle interaction energy, which allows the following identity:

$$\frac{1}{2}\sum_{i=1,i\neq 1}^{N}\sum_{j=1}^{N} v(|\mathbf{r}_i-\mathbf{r}_j|)=\frac{1}{2}\sum_{i=1,i\neq 1}^{N}\sum_{j=1}^{N} v(|\boldsymbol{\rho}_i-\boldsymbol{\rho}_j|), \quad (7)$$

where $\rho_{i(j)}=\sqrt{(x_i-x_j)^2+(x_i-y_j)^2}$.

The two-dimensional Hamiltonian will be written in the following form:

$$H^{2D}=H_0^{2D}+V_{\text{int}}^{2D}(\boldsymbol{\rho}_1,\ldots,\boldsymbol{\rho}_N). \quad (8)$$

F. Peeters, T. Chakraborty, and A. Madhav have shown that the non-interacting part of the Hamiltonian in the equation (6) can be exactly diagonalized and presented via the creation and annihilation operators, which are defined through these relations [18,19]:

$$A_{1,2}^{\pm}=\sum_{i=1}^{N} a_{1,2}^{\pm}(i),$$

$$a_{1,2}^{\pm}(i)=u_{1,2}\left[x_i\left(-\omega_{1,2}^2+\Omega_b^2+\frac{1}{2}\omega_c^2\right)\right.$$

$$\mp i\,\frac{p_{i,x}}{\mu\omega_{1,2}}\left(-\omega_{1,2}^2+\Omega_b^2\right)$$

$$\left.\mp iy_i\,\frac{\omega_c}{2\omega_{1,2}}\left(\omega_{1,2}^2+\Omega_b^2\right)-\frac{p_i}{\mu}\,\omega_c\right] \quad (9)$$

where $u_{1,2}=(\mu\omega_{1,2}/2\hbar)^{1/2}[(\omega_{1,2}^2-\Omega_b^2)^2+\omega_c^2\Omega_b^2]^{-1/2}$, with eigenfrequencies $\omega_{1,2}$ presented below:

$$\omega_{1,2}^2=\frac{1}{2}\left[\Omega_a^2+\Omega_b^2+\omega_c^2\pm\sqrt{(\Omega_a^2+\Omega_b^2+\omega_c^2)^2-4\Omega_a^2\Omega_b^2}\right] \quad (10)$$

F. Peeters also has shown that between these operators and the two-dimensional non-interacting Hamiltonian H_0^{2D} the interparticle interaction energy V_{int}^{2D} and the Hamiltonian of the interacting system H^{2D} the following commutation relations take place:

$$[H_0^{2D},A_{1,2}^{\pm}]=\pm\hbar\omega_{1,2}A_{1,2}^{\pm},$$

$$[V_{\text{int}}^{2D},A_{1,2}^{\pm}]=0, \quad (11)$$

$$[H^{2D},A_{1,2}^{\pm}]=[H_0^{2D}+V_{\text{int}}^{2D},A_{1,2}^{\pm}]=\pm\hbar\omega_{1,2}A_{1,2}^{\pm}.$$

Suppose the long-wave radiation falls on the system. In that case, the interaction of the particles with the electromagnetic field of incident radiation is described by the term H', which is added to the total Hamiltonian as a perturbation and is given by the following relation:

$$H'=-e\mathbf{E}(t)\sum_i\boldsymbol{\rho}_i$$

$$=-eE_0e^{-\imath\omega t}\left(\cos\theta\sum_{i=1}^{N}x_i+\sin\theta\sum_{i=1}^{N}y_i\right)$$

$$=-eNE_0e^{-i\omega t}(X\cos\theta+Y\sin\theta), \quad (12)$$

in the dipole approximation, where $\mathbf{E}(t)=$ $=E_0(\cos\theta,\sin\theta)e^{-i\omega t}$ is the electric field vector of the incident radiation, θ — the angle between the OX axis and $E(t)$ and $X(Y)=(1/N)\sum_{i=1}^{N}x_i(y_i)$ — the center of mass coordinates. Using the creation and annihilation operators $A_{1,2}^{\pm}$, shown above, the operator H' will be written in this form:

$$H'=-eE_0e^{-i\omega t}\left\{\xi_1\cos\theta\left[(A_1^-+A_1^+)-\frac{u_1}{u_2}(A_2^-+A_2^+)\right]\right.$$

$$\left.+\xi_2\sin\theta\left[(A_1^--A_1^+)-\frac{u_1}{u_2}\xi_3(A_2^--A_2^+)\right]\right\}, \quad (13)$$

where

$$X=\xi_1\left[(A_1^-+A_1^+)-\frac{u_1}{u_2}(A_2^-+A_2^+)\right],$$

$$Y=\xi_2\left[(A_1^--A_1^+)-\frac{u_1}{u_2}\xi_3(A_2^--A_2^+)\right], \quad (14)$$

with the following designations: $\xi_1=1/[2u_1(\omega_2^2-\omega_1^2)]$, $\xi_2=\omega_1(\Omega_d^2-\omega_2^2)/[2iu_1\omega_c\Omega_b^2(\omega_1^2-\omega_2^2)]$, and $\xi_3=\omega_2$ $\times(\Omega_b^2-\omega_1^2)/[\omega_1(\Omega_b^2-\omega_2^2)]$. From (13) follows that the action of the operator H' on the states described by the non-interacting Hamiltonian H_0^{2D}, as well as the Hamiltonian considering the pair-interaction, leads to the transitions with the same resonant frequencies in both cases, equal to ω_1, ω_2.

Thus, the long-wave intraband transitions for the pair-interacting heavy-hole gas are realized in the considered system, the resonant frequencies of which have a oneparticle character and don't depend on the number N of particles. This assertion is the generalized Kohn theorem.

Maksym and Chakraborty in [30] have investigated the model of a two-dimensional parabolic QD, containing a pair-interacting electron gas in the presence of an axial magnetic field. Based on numerical modeling, they have constructed an energy diagram for the considered system at various values of the magnetic field and the number of particles. It is clear that the many-particle Hamiltonian with the Coulomb term of interparticle interaction is not exactly solvable; therefore, it is investigated numerically. On the other hand, N.F. Johnson and M.C. Payne have shown that, in the presence of a magnetic field, an exact analytical solution for the energy expression of a pair-interacting charged gas localized in a circular two-dimensional parabolic well can be found. It is assumed in that case that Hooke's law describes the pair-interaction between the particles [31]:

$$V_{\text{int}}^{2D}(\boldsymbol{\rho}_i,\boldsymbol{\rho}_j)=2V_0-\frac{1}{2}\mu\Omega_0^2|\boldsymbol{\rho}_i-\boldsymbol{\rho}_j|^2 \quad (15)$$

where V_0 and Ω_0 are positive parameters and are defined by comparing of $V_{\text{int}}^{2D}(\boldsymbol{\rho}_i,\boldsymbol{\rho}_j)$ with the Coulomb potential.

The mentioned case will correspond to the model of the strongly oblate ellipsoidal QD with the circular cross-section, when for the semiaxes a and b we have this relation: $a=b$. In turn, for the frequencies Ω_a and Ω_b one obtains:

Table 1. Center of mass $(n_1^{\mathrm{CM}}, n_2^{\mathrm{CM}})$ and relative $(n_1^{\mathrm{rel}}, n_2^{\mathrm{rel}})$ motion energy levels changing in magnetic field for $N = 5$ particles gas, $\Omega_0 = 8.5 \cdot 10^{12}\,\mathrm{s}^{-1}$ interaction parameter and $a = b = 5a_B$, $c = 1a_B$

State	Center of Mass (in meV)		Relative (in meV)	
	Without Field	Field (0.5 T)	Without Field	Field (0.5 T)
1	(0, 1) = 16.237	(1, 0) = 1.7740	(0, 1) = 46.897	(1, 0) = 2.1352
2	(1, 0) = 16.237	(2, 0) = 3.5481	(1, 0) = 46.897	(2, 0) = 4.2704
3	(0, 2) = 32.475	(3, 0) = 5.3221	(0, 2) = 93.793	(3, 0) = 6.4051
4	(1, 1) = 32.475	(0, 1) = 148.62	(1, 1) = 93.793	(0, 1) = 1030.0
5	(2, 0) = 32.475	(1, 1) = 150.39	(2, 0) = 93.793	(1, 1) = 1032.2
6	(1, 2) = 48.712	(2, 1) = 152.16	(1, 2) = 140.69	(2, 1) = 1034.3
7	(2, 1) = 48.712	(0, 2) = 297.23	(2, 1) = 140.69	(0, 2) = 2060.1
8	(0, 3) = 48.712	(1, 2) = 299.01	(0, 3) = 140.69	(1, 2) = 2062.2
9	(3, 0) = 48.712	(0, 3) = 445.84	(3, 0) = 140.69	(0, 3) = 3090.1

$\Omega \equiv \Omega_a = \Omega_b = \pi\hbar/2\mu ac$ [26]. It should be noted that this model is related to the Moshinsky atom [27], where, similarly, pair-interacting particles localized in a parabolic quantum well, described by Hooke's law, are considered. So the twodimensional N — particle Hamiltonian will be written as:

$$H_{\mathrm{JP}}^{\mathrm{2D}} = \frac{1}{2\mu}\sum_i p_i^2 + \frac{1}{2}\mu\omega_0^2(B)\sum_i |\boldsymbol{\rho}_i|^2 + \sum_{i=1}^{N}\sum_{j=1}^{N} V_{\mathrm{int}}^{\mathrm{2D}}(\boldsymbol{\rho}_i, \boldsymbol{\rho}_j) + \frac{\omega_c}{2}\sum_i L_{z_i}, \qquad (16)$$

where $\omega_0^2(B) = \Omega^2 + \omega_c^2/4$.

Performing the calculations presented in the article [31], one obtains the system's energy spectrum:

$$E = E_0 + N_{\mathrm{A}_1}\hbar\left[\omega_0(B) - \frac{\omega_c}{2}\right] + N_{\mathrm{A}_2}\hbar\left[\omega_0(B) + \frac{\omega_c}{2}\right] + \sum_{i<j}\left[\alpha_{ij}\hbar\left(\omega - \frac{\omega_c}{2}\right) + \beta_{ij}\hbar\left(\omega + \frac{\omega_c}{2}\right)\right], \qquad (17)$$

where $E_0 = \hbar\omega_0(B) + (N-1)\hbar\omega + N(N-1)V_0$ is the ground state energy with $\omega = \left[\omega_0^2(B) - N\Omega_0^2\right]^{1/2}$. $N_{\mathrm{A}_1(\mathrm{A}_2)}$, $\alpha_{ij}(\beta_{ij})$ are positive integers.

The resonant frequencies $(\omega_)(B) \pm \omega_c/2)$ of the system's center of mass transitions and the frequencies $\omega_{1(2)}$ obtained above for the asymmetric case, coincide with each other $(\omega_0(B) \pm \omega_c/2 = \omega_{1(2)})$ in the case of the circular cross section $(a = b)$ of QD. Using the following values for material parameters: $a = b = 5a_B$, $c = 1a_B$, $a_B = 2\,\mathrm{nm}$, $\mu = 0.394m_0$, and the value $B = 0.1\,\mathrm{T}$ for the magnetic field, the performed calculations for $\omega_{1(2)}$, yield these numerical values $\omega_1 = 46 \cdot 10^{12}\,\mathrm{s}^{-1}$ and $\omega_2 = 46 \cdot 10^{1}2\,\mathrm{s}^{-1}$. Thus, indicating that the eigenfrequencies $\omega_{1(2)}$ indeed fall in the mid-infrared region of the electromagnetic spectrum.

Turn to the character of the center of mass energy levels. At $B = 0$ the system will be described in the framework of the two-dimensional circular oscillator. As is known, such a system possesses the hidden symmetry and is characterized by the SU(2) symmetry group [32]. As a result, the energy levels are degenerated, with the order of degeneracy:

$$G(N) = N + 1, \qquad (18)$$

when $N = N_{\mathrm{A}_1} + N_{\mathrm{A}_2}$. If we introduce the states of the first three excited levels $N = 1, 2, 3$ then for the corresponding values of energy, we'll obtain the results presented in Table 1. The states (1, 0) and (0, 1) are double degenerated, and 16.237 meV energy corresponds to them. The states (2, 0), (0, 2), and (1, 1) are three times degenerated, and the energy value 32.475 meV corresponds to them. Finally, the states (1, 2), (2, 1), (3, 0), and (0, 3) are degenerated four times, with corresponding to them 48.712 meV energy value. As can be seen in Table 1. The application of a magnetic field significantly alters the order of placement of levels. For example, the states (1, 0), (2, 0), (3, 0) are significantly going down, which is a direct consequence of the magnetic field (see the (17) formula), when $N_{\mathrm{A}_1} = 1; 2; 3$, $N_{\mathrm{A}_1} = 0$ and the cyclotron energy gives a negative contribution. In turn, the states (0, 1), (0, 2), and (0, 3) are significantly rising, which also follows from (17), when the contribution of the energy $\hbar\omega_c/2$ is already positive. It should be noted that such behavior is typical for the Fock–Darwin levels. Thus, the magnetic field removes the system's hidden symmetry, as well as creates the new order of placement of energy levels.

For the wave function of the system, one obtains [31]:

$$\Psi = (\mathrm{A}_1^+)^{N_{\mathrm{A}_1}}(\mathrm{A}_2^+)^{N_{\mathrm{A}_2}}\prod_{i<j}(a_{ij}^+)^{\alpha_{ij}}(b_{ij}^+)^{\beta_{ij}}\Psi_0. \qquad (19)$$

Here Ψ_0 is the wave function of the ground state and is defined by the following relation:

$$\Psi_0 = C_0 \exp\left[-\frac{N\mu\omega_0(B)}{2\hbar}(X^2+Y^2)\right] \times \exp\left[-\frac{\mu\omega}{2N\hbar}\sum_{i<j}(x_{ij}^2+y_{ij}^2)\right], \qquad (20)$$

where C_0 is the normalization constant, (X, Y) are the center of mass coordinates, and $(x_{i,j}, y_{ij})$ — the coordinates of the relative motion of particles.

The operators in the above expressions $A_1^+(A_2^+)$ and $a_{ij}^+(b_{ij}^+)$ describe the center of mass and the relative motion transitions, respectively. $A_1^-(A_2^-)$ and $a_{ij}^-(b_{ij}^-)$ are complex conjugates of the above-presented ones. The expressions of those operators are presented below [31]:

$$A_1^{\pm}=\left(\frac{1}{4N\mu\hbar\omega_0(B)}\right)^{1/2}\Big[N\mu\omega_0(B)(X\mp iY)\mp i(P_X\mp iP_Y)\Big],$$

$$A_2^{\pm}=\left(\frac{1}{4N\mu\hbar\omega_0(B)}\right)^{1/2}\Big[N\mu\omega_0(B)(X\pm iY)\mp i(P_X\pm iP_Y)\Big],$$

$$a_{ij}^{\pm}=\left(\frac{1}{4\mu\hbar\omega}\right)^{1/2}\Big[\mu\omega(x_{ij}\mp iy_{ij})\mp i(p_{x,ij}\mp ip_{y,ij})\Big],\ i\neq j$$

$$b_{ij}^{\pm}=\left(\frac{1}{4\mu\hbar\omega}\right)^{1/2}\Big[\mu\omega(x_{ij}\pm iy_{ij})\mp i(p_{x,ij}\pm ip_{y,ij})\Big]. \qquad (21)$$

It should be noted that these operators satisfy rather complicated commutation relations given in [31].

3. Results

Before we discuss the results, we note that the case of the strongly oblate ellipsoidal QD made of Ge/Si has been considered. For the numerical simulation, we took the dot material as Ge_xSi_{1-x} solid solution with Ge about 60 %. The material parameters which have been used in the calculations are the following: hole effective mass $\mu = 0.394m_0$ where m_0 is the free electron mass, dielectric constant $e_r = 14.4$ and Bohr radius $a_B = 2$ nm. In the interaction potential (15) we considered, we have two main interaction parameters, V_0 and Ω_0 by adjusting which we can control the interaction strength. In this case, we fixed the value of the first parameter V_0 in accordance with the article (31) and varied the second parameter Ω_0 by numerically equating this interaction potential to the Coulomb ones. It is clear that the parameter Ω_0 strongly depends on the interparticle distance, and for example, for an interparticle distance of 4 n, $V_0 = 10$ meV, $\hbar\Omega_0 = 6$ meV, and $\Omega_0 + 8.5\cdot 10^{12}\,\mathrm{s}^{-1}$.

In Figure 2, the center of mass energy dependencies on the geometrical parameters (semi-axes a and c) of the QD, as well as the magnitude of the magnetic field$B$, are presented. Figure 2, *a* shows the dependencies of the center of mass energy on the magnetic field and the small semi-axis c of QD, for state $N_{A_1} = 1$, $N_{A_2} = 0$)and fixed semi-axis $a = 5c(c = a_B)$. As one can see in the figure, the increase of B leads to the decrease of the energy values, which corresponds to the energy spectrum (17), for the (1, 0) state. At the same time, E_{CM} decreases with the increase of parameter although at $B = 0$ T, this dependence is more pronounced compared to the case when $B = 1$ T. Figure 2, *b* presents the same dependencies as Figure 2, *a* for the state (0, 1) at fixed semi-axis $a = 5c$. Again, referring to expression (17), one can see that the energy should almost linearly increase with the magnetic field, which is the case. At the same time, this dependence is more pronounced compared to the one with the semi-axis However, the small decrement of energy values can be seen with the increasing parameter c. The dependencies in Figure 2, *c* are obtained for the state (1, 0), in the absence of B. As can be seen from the figure, energy decreases with the increase in both parameters a and c. At the same time, one can also notice that the dependence is stronger in the case of the small semi-axis c which is a consequence of the weakening of the size quantization regime in the axial direction. The latter circumstance leads to a sharp decrease in energy values. Figure 2, *d* is obtained for the same dependencies as Figure 2, *c*, but already in the presence of an axial magnetic field B equal to).5 T. It can be noticed here that the overall energy values are smaller than those in Figure 2, *c*. This is explained by the fact that for the state (1, 0), in the presence of a magnetic field, the energy decreases by the amount $\hbar\omega_c/2$ as can be seen in the relation (17). Nevertheless, the energy values are also decreasing with the increase of geometrical parameters, similar to Figure 2, *c*.

In Figure 3, the relative motion energy dependencies on the magnetic field B particles' number N as well as the interparticle interaction parameter Ω_0 for the fixed geometrical parameters $(a = b = 5a_B, c = a_B)$ are shown. Figure 3, *a* presents the relative motion energy dependencies on B and N for the state (1, 0) and fixed interaction parameter Ω_0 equal to $8.5\cdot 10^{12}\,\mathrm{s}^{-1}$. From the term describing the relative motion in the formula (17), one can see that for the state (1, 0), the energy values should decrease with the increase of the magnetic field, which is actually observed in the figure. On the other hand, the energy increases with N, which is explained by the contribution of each particle to the increase of the system's total energy. The same dependencies are shown in Figure 3, *b* for the state (0, 1). Unlike Figure 3, *a*, the energy increases with the increase of the magnetic field, which is also in correspondence with (17). In this case, similar to Figure 3, *a*, the increase of N leads to an increase in energy values. Furthermore, it can be noticed here that the particles' number N has a greater influence on the energy states than B. In Figure 3, *c* are presented the dependencies of E_{rel} on the magnetic field B and the interaction parameter Ω_0 for the state (0, 1), at a fixed number of particles ($N = 5$). It can be seen from the figure that the increase in Ω_0 only slightly decreases the energy values, unlike the magnetic field, with the increase of which E_{rel} increases almost linearly. For the same (0, 1)

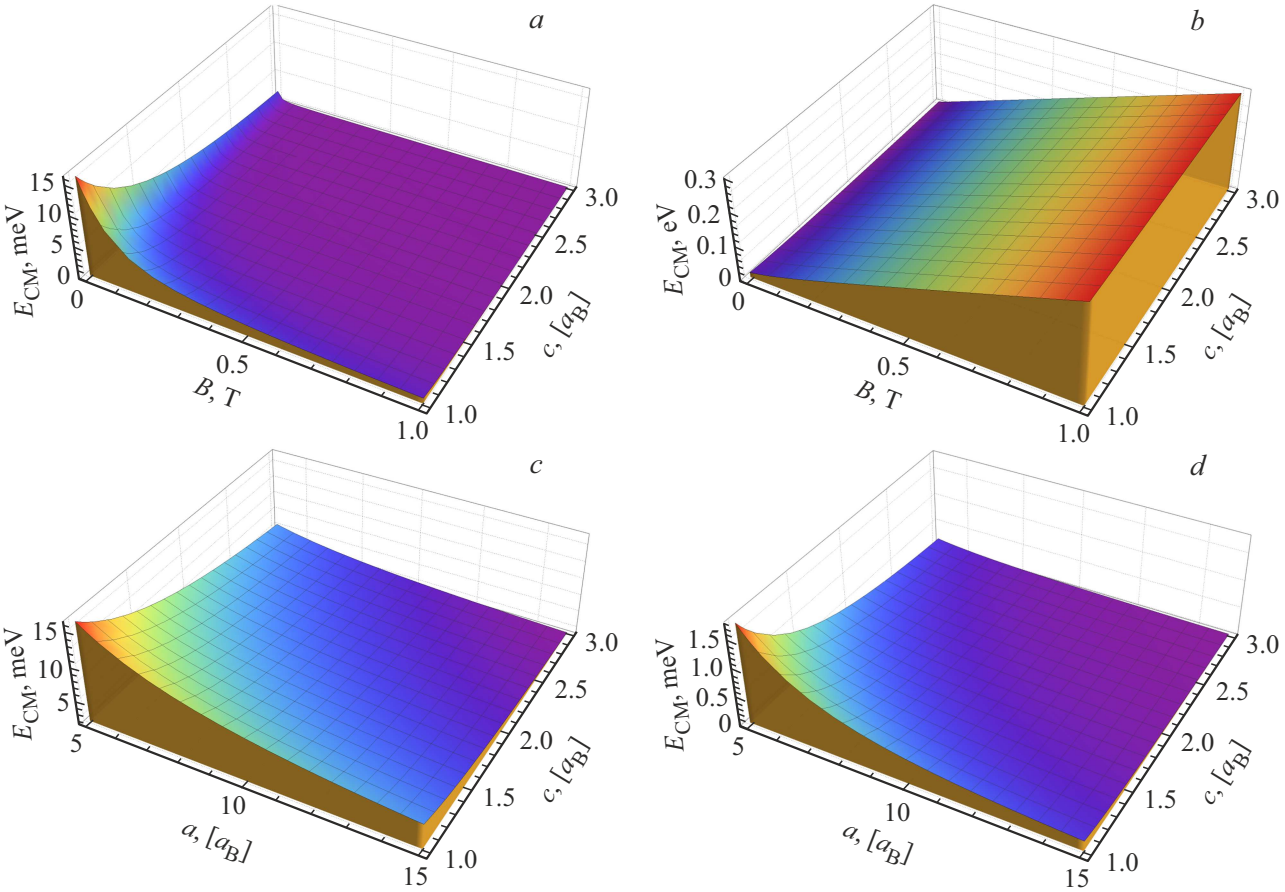

Figure 2. Hole gas center of mass motion energy dependencies from (a) — magnetic field B and semi-axis c for (1, 0) state and $a = 5c$ semi-axis, (b) — magnetic field B and semi-axis c for (0, 1) state and $a = 5c$ semi-axis, (c) — a and c semi-axes for (1, 0) state and without magnetic field, (d) — a and c semi-axes for (1, 0) state and $B = 0.5\,\mathrm{T}$ magnetic field.

state the dependencies of E_{rel} on Ω_0 and the particles' number N for the constant magnetic field ($B = 0.5\,\mathrm{T}$) are shown in Figure 3, d. Similar to Figure 3, cc the influence of the interaction parameter Ω_0 on relative motion energy states are negligibly small. At the same time, the increase of N leads to a sharp increase in the values of the relative motion energies. All the presented dependencies follow from the expression (17), obtained for the energy spectrum.

In Figure 4, the relative motion energy diagrams are shown for two cases, when $B = 0\,\mathrm{T}$ and $B = 0.5\,\mathrm{T}$ at fixed interaction parameter $\Omega_0 = 8.5 \cdot 10^{12}\,\mathrm{s}^{-1}$. The following three states are chosen: (0, 1), (1, 1), (2, 1). As one can notice, in the case of $B = 0\,\mathrm{T}$, both the distances between the energy levels and their absolute values increase with the increase of particles' number N in the system, as each particle contributes to the increase of the system's total energy. However, in the case of a non-zero magnetic field, the distances between energy levels decrease, as can be seen from expression (17), which indicates that the magnetic field acts differently on the states presented in the figure. Here again, independently of the distances between the levels, the absolute values of energy increase with N the reason for which is the same as in the case with zero field.

The combined energy diagrams of both the center of mass states and the relative motion states are presented in Figure 5, for different values of particles' number N, and the interaction constant Ω_0. Figure 5, a shows the relative motion energy level (0, 1) with those of the system's center of mass, for the interacting two-particle system in the presence of an axial magnetic field equal to $B = 0.1\,\mathrm{T}$ and interaction constant $\Omega_0 = 8.5 \cdot 10^{12}\,\mathrm{s}^{-1}$, while in Figure 5, b, $N = 4$ at the same values of B and Ω_0. Comparing Figure 5, a and Figure 5, b, we can see that with the increase in particles' number N in the system, the value of the relative motion energy for the state (0, 1) increases. It is already mentioned earlier that the increase in N causes an increase in the relative motion energy values, which is the case. At the same time, the difference between the center of mass energy values remains unchanged with respect to that in Figure 5, a. In the case of the non-interacting system of four particles under an axial magnetic field, shown in Figure 5, c, the (0, 1) state value slightly increases. This takes place due to the elimination of the interaction parameter Ω_0 from the (17) formula. However, here also the difference between the center of mass energy levels is equal to those in the cases of 5, a and 5, b. The conclusion that can be made, thus, is that the center of

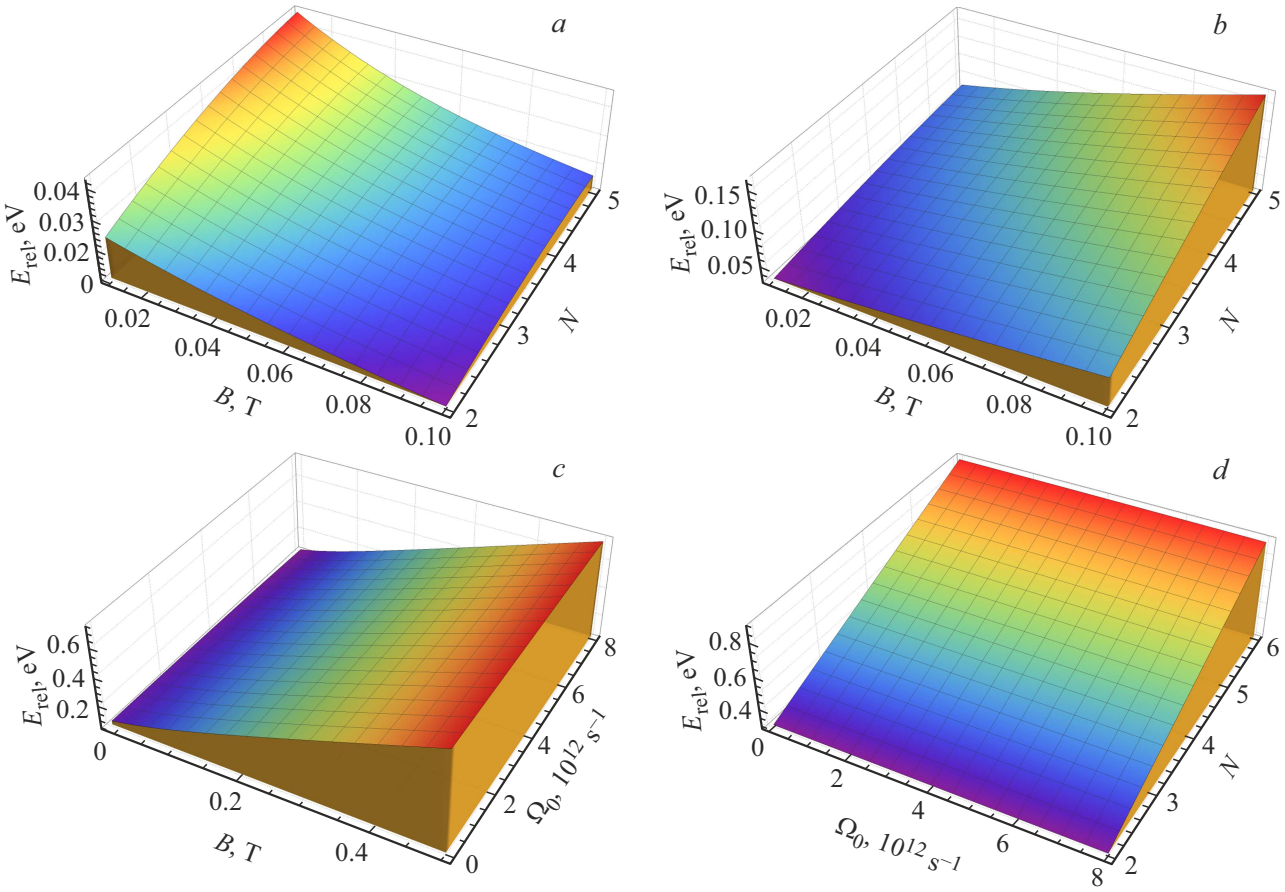

Figure 3. Hole gas relative motion energy dependencies for $a = b = 5a_B$ and $c = a_B$ geometry from (a) — magnetic field B and particles number N for (1, 0) state and interaction parameter $\Omega_0 = 8.5 \cdot 10^{12}\,\mathrm{s}^{-1}$, ($b$) — magnetic field B and particles number N for (0, 1) state and interaction parameter $\Omega_0 = 8.5 \cdot 10^{12}\,\mathrm{s}^{-1}$, ($c$) — magnetic field B and interaction parameter Ω_0 for particles number $N = 5$ and (0, 1) state, (d) — interaction parameter Ω_0 and particles number N for magnetic field $B = 0.5\,\mathrm{T}$ and (0, 1) state.

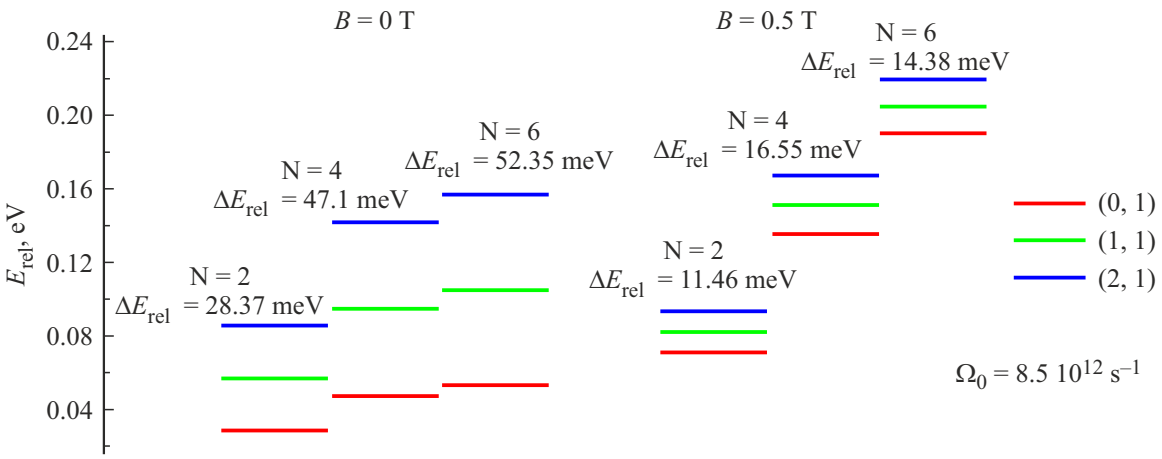

Figure 4. Hole gas relative motion 3-levels energy diagrams for $B = 0$ and $B = 0.5\,\mathrm{T}$ different magnetic fields and $N = \{2, 4, 6\}$ different numbers of particles in QD for constant interparticle interaction frequency $8.5 \cdot 10^{12}\,\mathrm{s}^{-1}$.

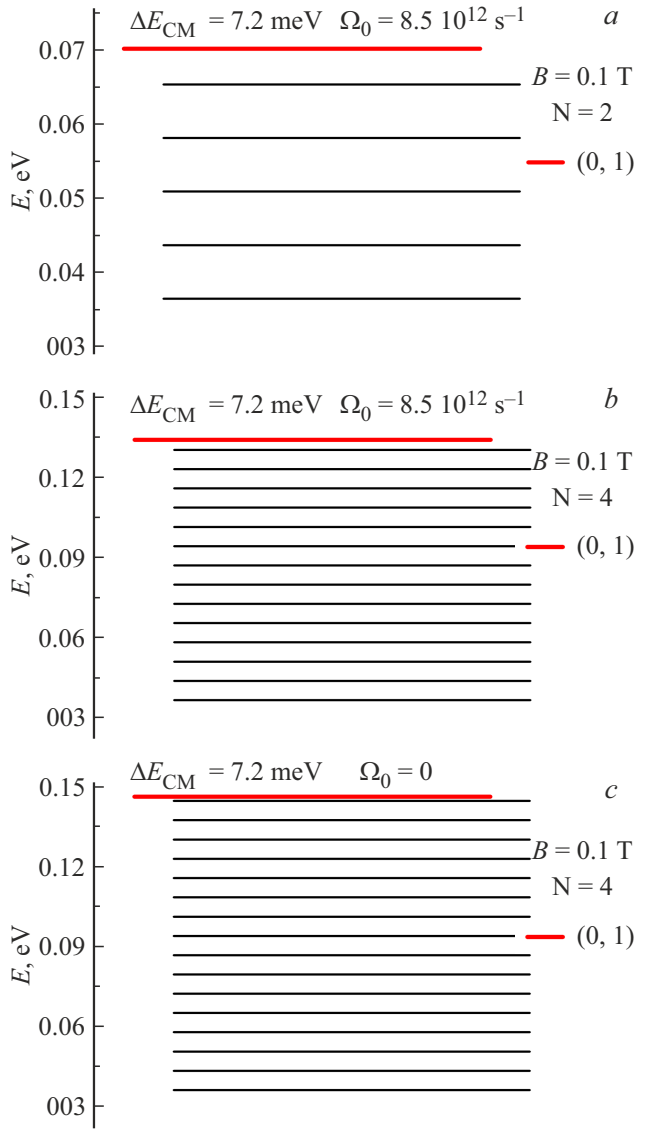

Figure 5. Hole gas total energy diagrams where one levels of relative motion correspond to a family of levels of the center of mass (black lines) for (a) — particle number $N = 2$, magnetic field $B = 0.1\,\mathrm{T}$ and interaction parameter $\Omega_0 = 8.5 \cdot 10^{12}\,\mathrm{s}^{-1}$, ($b$) — particle number $N = 4$, magnetic field $B = 0.1\,\mathrm{T}$ and interaction parameter $\Omega_0 = 8.5 \cdot 10^{12}\,\mathrm{s}^{-1}$, ($c$) — particle number $N = 4$, magnetic field $B = 0.1\,\mathrm{T}$ and without interaction.

mass transitions are independent of both the number N in the system and the interaction between them. This phenomenon is evidence of the fulfillment of the generalized Kohn theorem in the considered system.

4. Conclusion

Summarizing, the following can be said: that the generalized Kohn theorem can be realized in the asymmetric and circular symmetrical strongly oblate ellipsoidal QDs in the presence of an axial magnetic field. The calculations based on the adiabatic method show that in the case of a strongly oblate asymmetric ellipsoidal Ge/Si QD, containing heavy hole gas, the slow subsystem is described in the framework of a pair-interacting gas, localized in the asymmetric two-dimensional parabolic well with the frequencies Ω_a and Ω_b. At the same time, the resonant frequencies of the long-wave transitions between the hole gas center of mass levels are characterized by both the two-dimensional confining potential frequencies and the cyclotron frequency conditioned by the magnetic field. In the case of the ellipsoidal QD with circular symmetry, when $\Omega_a = \Omega_b$, the oscillator interaction approximation between the holes can be used. In that case, the problem is reduced to describing the behavior of the hole gas with oscillator pair-interaction, localized in a two-dimensional circular parabolic well, in the presence of an axial magnetic field. Johnson and Payne showed that such a problem is exactly solvable. Based on that, the energy diagrams of the hole gas are constructed, and the realization of the generalized Kohn theorem is demonstrated in the explicit form in that system. Besides that, the resonant frequencies for QDs with both the asymmetric and circular symmetry can be manipulated by the change of their geometrical parameters. The numerical estimations indicate that the resonant frequencies of the long-wave transitions fall within the terahertz region. In particular, for $a = b = 5c$, $c = a_B$, and $B = 0.1\,\mathrm{T}$ for the resonant frequency ω_{res} one obtains $46 \cdot 10^{12}\,\mathrm{s}^{-1}$.

5. Acknowledgement

A.A.N., M.A.M., and H.A.S. express their gratitude to the Committee on Higher Education and Science of the Ministry of Education, Science, Culture, and Sports of the Republic of Armenia for their support.

M.Ya.V. and D.A.F. thank the Ministry of Science and Higher Education of the Russian Federation (state assignment for basic research FSEG-2023-0016) for financial support.

Special thanks to Professor S. Dabagov for valuable discussions during the writing of this article.

References

[1] S.M. Reimann, M. Manninen. Electronic structure of quantum dots, Reviews of modern physics **74** (4), 1283 (2002).
[2] Y. Alhassid. The statistical theory of quantum dots, Reviews of Modern Physics **72** (4), 895 (2000).
[3] L. Jacak, P. Hawrylak, A. Wojs. Quantum dots, Springer Science & Business Media, 2013.
[4] U. Woggon. Optical properties of semiconductor quantum dots, Springer, 1997.
[5] V.M. Galitsky, B.M. Karnakov, V.I. Kogan. Problems in Quantum Mechanics: Textbook., M.: Science, the Main edition of physical and mathematical literature, 1981.
[6] D. Bimberg, M. Grundmann, N.N. Ledentsov. Quantum dot heterostructures, John Wiley & Sons, 1999.
[7] T. Chakraborty. Quantum Dots: A survey of the properties of artificial atoms, Elsevier, 1999.

[8] H. Alehdaghi, E. Assar, B. Azadegan, J. Baedi, A.A. Mowlavi. Investigation of optical and structural properties of aqueous CdS quantum dots under gamma irradiation, Radiation Physics and Chemistry **166**, 108476 (2020).
[9] O.D. Bekasova, A.A. Revina, A.L. Rusanov, E.S. Kornienko, B.I. Kurganov. Effect of gamma-ray irradiation on the size and properties of CdS quantum dots in reverse micelles, Radiation Physics and Chemistry **92**, 87–92, (2013).
[10] K. Khachatryan, M. Mkrtchyan, D. Hayrapetyan, S. Baskoutas, C. Garoufalis, C. Duque, H. Sarkisyan. Temperature influence on interband and intraband optical transitions in pyramidal quantum dot, The European Physical Journal Plus **140** (9), 909 (2025).
[11] Z. Li, L. Peng, Y. Fang, Z. Chen, D. Pan, M. Wu. Synthesis of colloidal SnSe quantum dots by electron beam irradiation, Radiation Physics and Chemistry **80** (12), 1333–1336 (2011).
[12] I.V. Ignatiev, I.E. Kozin, H.-W. Ren, Sh. Sugou, Y. Masumoto. Anti-Stokes photoluminescence of InP self-assembled quantum dots in the presence of electric current, Physical review B **60** (20), R14001 (1999).
[13] G. Yu, S. Lian-Liang, C. Feng. Heat generation by electric current in a quantum dot molecular coupled to ferromagnetic leads, Communications in Theoretical Physics **62** (3), 423 (2014).
[14] J. Liu, J. Song, Q.-f. Sun, X.C. Xie. Electric-current-induced heat generation in a strongly interacting quantum dot in the Coulomb blockade regime, Physical Review B–Condensed Matter and Materials Physics **79** (16), 161309 (2009).
[15] K.J. Mintz, Y. Zhou, R.M. Leblanc. Recent development of carbon quantum dots regarding their optical properties, photoluminescence mechanism, and core structure, Nanoscale **11** (11), 4634–4652 (2019).
[16] I. Moreels, K. Lambert, D. Smeets, D. De Muynck, T. Nollet, J.C. Martins, F. Vanhaecke, A. Vantomme, C. Delerue, G. Allan, Z. Hens, Size-dependent optical properties of colloidal PbS quantum dots, ACS nano **3** (10), 3023–3030 (2009).
[17] Y. Léger, L. Besombes, L. Maingault, D. Ferrand, H. Mariette. Geometrical Effects on the Optical Properties of Quantum Dots Doped format with a Single Magnetic Atom, Physical review letters —bf95 (4), 047403 (2005).
[18] F.M. Peeters. Magneto-optics in parabolic quantum dots, Physical Review B **42** (2), 1486 (1990).
[19] A.V. Madhav, T. Chakraborty. Electronic properties of anisotropic quantum dots in a magnetic field. Physical Review B **49** (12), 8163 (1994).
[20] A.O. Govorov, A.V. Chaplik. Magnetoabsorption at quantum points, JETP Lett., **52** (1), 681–683 (1990).
[21] W. Kohn. Cyclotron resonance and de Haas-van Alphen oscillations of an interacting electron gas. Physical Review **123** (4), 1242 (1961).
[22] D.B. Hayrapetyan, E.M. Kazaryan, H.A. Sarkisyan. Implementation of Kohn's theorem for the ellipsoidal quantum dot in the presence of external magnetic field, Physica E: Low-dimensional Systems and Nanostructures **75**, 353–357 (2016).
[23] H.A. Sarkisyan, D.B. Hayrapetyan, L.S. Petrosyan, E.M. Kazaryan, A.N. Sofronov, R.M. Balagula, D.A. Firsov, L.E. Vorobjev, A.A. Tonkikh. Realization of the Kohn's theorem in Ge/Si quantum dots with hole gas: Theory and experiment, Nanomaterials **9** (1), 56 (2019).
[24] M.A. Mkrtchyan, D.B. Hayrapetyan, E.M. Kazaryan, H.A. Sarkisyan, S. Baskoutas, D.A. Firsov, M.Ya. Vinnichenko. One-and few-particle optics of the valence band in lens-shaped Ge/Si quantum dots, Physica E: Low-dimensional Systems and Nanostructures **150**, 115703 (2023).
[25] R.V. Ustimenko, M.Ya. Vinnichenko, D.A. Karaulov, H.A. Sarkisyan, D.B. Hayrapetyan, D.A. Firsov. Effect of Doping and Interband Pumping on the Optical Properties of GeSi/Si Quantum Dot Nanostructures for Infrared Detectors, ACS Applied Nano Materials **7** (23), 27245–27253, (2024).
[26] A.A. Nahapetyan, M.A. Mkrtchyan, Y.Sh. Mamasakhlisov, M.Ya. Vinnichenko, D.A. Firsov, H.A. Sarkisyan. Few-particle gas in strongly oblate asymmetric ellipsoidal quantum dot, Nuclear Instruments and Methods in Physics Research Section A: Accelerators, Spectrometers, Detectors and Associated Equipment **1073**, 170251 (2025).
[27] M. Moshinsky. How Good is the Hartree-Fock Approximation, American Journal of Physics **36** (1), 52–53 (1968).
[28] M.A. Mkrtchyan, Y.Sh. Mamasakhlisov, D.B. Hayrapetyan, S. Baskoutas, H.A. Sarkisyan. Two-dimensional pair-interacting hole gas thermodynamics: Exactly solvable moshinsky model for lens-shaped quantum dots, Heliyon **10** (15) (2024).
[29] D.B. Hayrapetyan, E.M. Kazaryan, M.A. Mkrtchyan, H.A. Sarkisyan. Longwave absorption of Few-Hole gas in prolate ellipsoidal Ge/Si quantum dot: implementation of analytically solvable Moshinsky model, Nanomaterials **10** (10), 1896 (2020).
[30] P.A. Maksym, T. Chakraborty. Quantum dots in a magnetic field: Role of electron-electron interactions, Phys. Rev. Lett. **65**, 108–111 (1990).
[31] N.F. Johnson, M.C. Payne. Exactly solvable model of interacting particles in a quantum dot, Phys. Rev. Lett. **67**, 1157–1160 (1991).
[32] J.P. Elliott, P.G. Dawber. Symmetry in Physics: Principles and Simple Applications, MacMillan Press, 1979.